Program Digest, 2019 IEEE International Ultrasonics Symposium (IUS)
Glasgow, Scotland, October 6-9, 2019

Iterative Retrospective Recovery of Full Synthetic Aperture Data from Focused Transmissions

Rehman Ali
Department of Electrical Engineering
Stanford University
Stanford, CA
rali8@stanford.edu

Jeremy J. Dahl
Department of Radiology
Stanford School of Medicine
Stanford, CA
jjdahl@stanford.edu

Nick Bottenus
Department of Biomedical Engineering
Duke University
Durham, NC
nick.bottenus@duke.edu

***Abstract*—Retrospective Encoding For Conventional Ultrasound Sequences (REFoCUS) enables recovery of the full-synthetic aperture (FSA) dataset from focused transmits while avoiding the drawbacks of single- and virtual-element transmissions. It was recently shown that a regularized inversion approach significantly improves the accuracy of the recovered FSA dataset over the REFoCUS method when applied to a walking-aperture transmit sequence. However, this approach becomes computationally burdensome when applied to walking aperture sequences on larger linear arrays. We present an iterative form of REFoCUS that improves FSA dataset recovery to better handle these cases.**

***Index Terms*—Synthetic Aperture, Forward-Adjoint Oracles, Matrix-Free Optimization, Conjugate Gradient**

I. Introduction

Ultrasound images on commercial ultrasound systems are typically generated from channel data acquired from a set of focused transmissions. These systems apply dynamic-receive focusing to channel data from each transmit beam in order to form A-lines in the ultrasound image. Virtual source synthetic aperture imaging techniques employ a set of parallel imaging lines for each transmit beam in order to improve transmit focusing in the image [1]. However, because this image formation approach requires accurate characterization of the spatial profile of the transmit beam as it propagates through space and can introduce a discontinuity artifact at the focal depth. Because virtual source synthetic aperture relies on entire transmit beams for image reconstruction, imaging quality is mainly limited by assumptions made about sound speed in the medium during the transmit beamforming process. Furthermore, in the presence of sound speed errors and phase aberration, it becomes difficult to accurately place the wavefront for the focused transmit beam.

Recent works [2]–[4] have shifted their focus away from virtual source synthetic aperture towards the recovery of the full-synthetic aperture (FSA) dataset. Since the FSA dataset consists of receive channel data from individual transmit elements, the weights and delays applied to each individual element can be flexibly adjusted to account for phase aberration induced by sound speed inhomogeneity in the medium. As a result, recovery of the FSA dataset and subsequent focusing of channel data can result in optimal focusing (diffraction limited resolution) at all points in the image. Retrospective Encoding for Conventional Ultrasound Sequences (REFoCUS) [2] was initially proposed for recovering the FSA dataset by summing transmit beam data that has been delayed to align at each individual transmit element. This approach was shown to be mathematically adjoint to the transmit beamforming process. Because the adjoint no longer approximates the inverse for the walking aperture transmit sequence, regularized inversion was also investigated for FSA dataset recovery [3].

This work proposes an iterative scheme for recovering the FSA dataset by pairing the transmit beamforming (forward) process with REFoCUS (adjoint) to form a forward-adjoint oracle (FAO) [5]. We pose FSA dataset recovery as a least-squares problem so that FSA channel data may be recovered by using the conjugate gradient (CG) algorithm. Although regularized inversion significantly improves the accuracy of the recovered FSA dataset for walking-apertures transmit sequences [3], regularized inversion becomes computationally burdensome when applied to large linear arrays that additionally require walking receive apertures. We present an iterative technique that generalizes FSA dataset recovery to better handle these challenging cases.

II. Theory

A. Forward Model for Transmit Beamforming

We denote $u_{TR}(t)$ as the full-synthetic aperture dataset indexed by transmit element $T \in [1, ..., N_{elem}]$ and receive element $R \in [1, ..., N_{elem}]$. The received channel data $s_{nR}(t)$ from transmit beam $n \in [1, ..., N_{beams}]$ can computed from the full-synthetic aperture dataset by the delay-and-sum formula

$$s_{nR}(t) = \sum_{T=1}^{N_{elem}} w_{nT} u_{TR}(t - \tau_{nT}), \tag{1}$$

where τ_{nT} and w_{nT} are the delay and apodization applied to transmit element T in constructing transmit beam n. Taking a Fourier-transform of this delay-and-sum equation yields

$$S_{nR}(f) = \sum_{T=1}^{N_{elem}} A_{nT}(f) U_{TR}(f) \tag{2}$$

where $A_{nT}(f) = w_{nT} e^{-j2\pi f \tau_{nT}}$. Indexed over all transmit beams, this summation can be written as a system of linear

equations, which can be concisely written as the matrix-vector product

$$\boldsymbol{S}_R(f) = \boldsymbol{A}(f)\boldsymbol{U}_R(f) \tag{3}$$

where $\boldsymbol{U}_R(f) \in \mathbb{C}^{N_{elem}}$, $\boldsymbol{A}(f) \in \mathbb{C}^{N_{beams} \times N_{elem}}$, and $\boldsymbol{S}_R(f) \in \mathbb{C}^{N_{beams}}$.

B. REFoCUS: the Adjoint of Transmit Beamforming

REFoCUS [2] proposes to recover an estimate $\hat{\boldsymbol{U}}_R(f)$ of the FSA dataset by applying the adjoint of $\boldsymbol{A}(f)$ to $\boldsymbol{S}_R(f)$, the set of focused transmit beams, at each frequency f:

$$\hat{\boldsymbol{U}}_R(f) = \boldsymbol{A}^*(f)\boldsymbol{S}_R(f) = [\boldsymbol{A}^*(f)\boldsymbol{A}(f)]\boldsymbol{U}_R(f). \tag{4}$$

The time-domain equivalent of this operation is the following time-advance and sum formula:

$$\hat{u}_{TR}(t) = \sum_{n=1}^{N_{beams}} w_{nT} s_{nR}(t + \tau_{nT}). \tag{5}$$

If $\boldsymbol{A}^*(f)\boldsymbol{A}(f)$ were the identity matrix, the FSA dataset would be recovered exactly. However, as shown previously in [3], $\boldsymbol{A}^*(f)\boldsymbol{A}(f)$ can be far from the identity matrix for certain transmit sequences. This observation initially motivated using regularized inversion as a pseudoinverse rather than the adjoint. However, regularized inversion offers no time-domain equivalent implementation and can be costly to implement for a large linear array with walked transmit and receive apertures. Rather than determine a closed-form inversion, the following section shows an iterative reconstruction scheme that uses transmit beamforming and REFoCUS as its mathematical adjoint.

C. Iterative Forward-Adjoint Reconstruction

Algorithm 1 summarizes the implementation of the CG-based iterative REFoCUS algorithm in the frequency domain. All matrix-vector multiplications involved in the CG algorithm use $\boldsymbol{A}(f)$ and its adjoint $\boldsymbol{A}^*(f)$. When Algorithm 1 translated to the time domain implementation shown in Algorithm 2, each instance of $\boldsymbol{A}(f)$ and $\boldsymbol{A}^*(f)$ is replaced by the delay-and-sum (1) and advance-and-sum (5), respectively.

Algorithm 1 Iterative REFoCUS in the Frequency Domain

$\boldsymbol{q}_R^0(f) = \boldsymbol{A}(f)\hat{\boldsymbol{U}}_R^0(f) - \boldsymbol{S}_R(f)$
$\boldsymbol{p}_R^0(f) = \boldsymbol{r}_R^0(f) = \boldsymbol{A}^*(f)\boldsymbol{q}_R(f)$,
for $k = 0, ..., K-1$ **do**
  $\boldsymbol{v}_R^k(f) = \boldsymbol{A}(f)\boldsymbol{p}_R^k(f)$
  $\alpha_R^k(f) = \|\boldsymbol{r}_R^k(f)\|_2^2 / \|\boldsymbol{v}_R^k(f)\|_2^2$
  $\hat{\boldsymbol{U}}_R^{k+1}(f) = \hat{\boldsymbol{U}}_R^k(f) + \alpha_R^k(f)\boldsymbol{p}_R^k(f)$
  $\boldsymbol{q}_R^{k+1}(f) = \boldsymbol{q}_R^k(f) + \alpha_R^k(f)\boldsymbol{v}_R^k(f)$
  $\boldsymbol{r}_R^{k+1}(f) = \boldsymbol{A}^*(f)\boldsymbol{q}_R^{k+1}(f)$
  $\beta_R^k(f) = \|\boldsymbol{r}_R^{k+1}(f)\|_2^2 / \|\boldsymbol{r}_R^k(f)\|_2^2$
  $\boldsymbol{p}_R^{k+1}(f) = -\boldsymbol{r}_R^{k+1}(f) + \beta_R^k(f)\boldsymbol{p}_R^k(f)$
end for
return $\hat{\boldsymbol{U}}_R^K(f)$

Algorithm 2 Iterative REFoCUS in the Time Domain

$q_{nR}^0(t) = -s_{nR}(t) + \sum_{T=1}^{N_{elem}} w_{nT}\hat{u}_{TR}^0(t - \tau_{nT})$
$p_{TR}^0(t) = r_{TR}^0(t) = \sum_{n=1}^{N_{beams}} w_{nT} q_{nR}^0(t + \tau_{nT})$,
for $k = 0, ..., K-1$ **do**
  $v_{nR}^k(t) = \sum_{T=1}^{N_{elem}} w_{nT} p_{TR}^k(t - \tau_{nT})$
  $\alpha_R^k(t) = \sum_{T=1}^{N_{elem}} (r_{TR}^k(t))^2 / \sum_{n=1}^{N_{beams}} (v_{nR}^k(t))^2$
  $\hat{u}_{TR}^{k+1}(t) = \hat{u}_{TR}^k(t) + \alpha_R^k(t) p_{TR}^k(t)$
  $q_{nR}^{k+1}(t) = q_{nR}^k(t) + \alpha_R^k(t) v_{nR}^k(t)$
  $r_{TR}^{k+1}(t) = \sum_{n=1}^{N_{beams}} w_{nT} q_{nR}^{k+1}(t + \tau_{nT})$
  $\beta_R^k(t) = \sum_{T=1}^{N_{elem}} (r_{TR}^{k+1}(t))^2 / \sum_{T=1}^{N_{elem}} (r_{TR}^k(t))^2$
  $p_{TR}^{k+1}(t) = -r_{TR}^{k+1}(t) + \beta_R^k(t) p_{TR}^k(t)$
end for
return $\hat{\boldsymbol{u}}_{TR}^K(t)$

III. Methods

A. Field II Simulation

Field II was used to simulate the complete FSA dataset for a diffuse-scattering medium whose reflectivities were modified to simulate a +6 dB hyperechoic lesion at 10 mm depth, a +12 dB hyperechoic lesion at 20 mm depth, and an anechoic lesion at 30 mm depth, all with 2 mm radius. The Field II simulation used a 96-element linear array with 0.154 mm pitch, and transmit pulse with 5 MHz center frequency and 70% fractional bandwidth. The sound speed in the medium is 1540 m/s and the sampling frequency of the channel data is 100 MHz. Receive channel data for focused transmit beams were simulated from the FSA dataset by using equation (1). The delays for the focused transmit beams in the walking aperture transmit sequence are

$$\tau_{nT} = \frac{1}{c}\left\{\sqrt{x_n^2 + z_n^2} - \sqrt{(x_T - x_n)^2 + z_n^2}\right\}, \tag{6}$$

where (x_n, z_n) is the transmit focus, $(x_n, 0)$ is the beam origin, and $(x_T, 0)$ are the coordinates of the transmit element T. Each transmit beam, focused at 30 mm depth, is emitted by an 8 mm rectangular walking aperture that translates from -3.65 to 3.65 mm in 0.05 mm steps.

B. Measurement of FSA Dataset Recovery

To monitor the recovery of FSA dataset at each iteration of CG, correlation is measured between the true and the recovered FSA datasets:

$$\rho = \frac{\mathrm{COV}[\hat{u}_{TR}, u_{TR}]}{\sqrt{\mathrm{COV}[\hat{u}_{TR}, \hat{u}_{TR}] \cdot \mathrm{COV}[u_{TR}, u_{TR}]}}. \tag{7}$$

Time-gain compensation is applied to both the recovered and true FSA datasets in order to adjust for the geometric spreading of the acoustic wave:

$$\mathrm{COV}[\hat{u}_{TR}, u_{TR}] = \int_{-\infty}^{\infty} t^2 \left(\sum_{T,R=1}^{N_{elem}} \hat{u}_{TR}(t) u_{TR}(t) \right) dt. \tag{8}$$

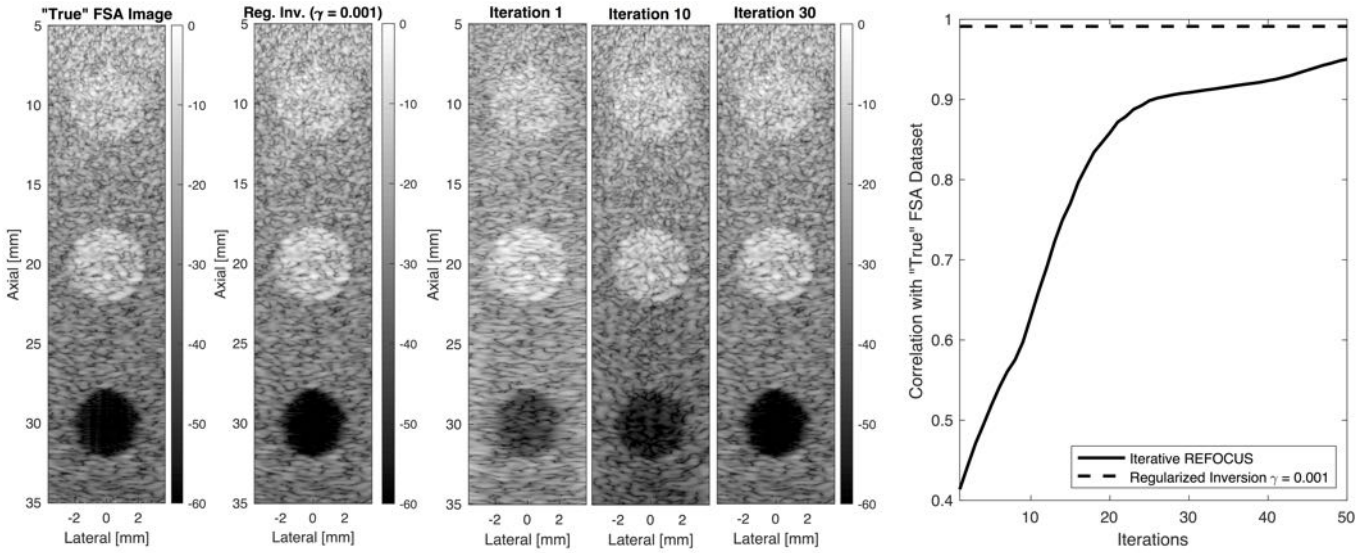

Fig. 1. Recovery of the FSA dataset at each iteration of CG. The first panel shows an image reconstructed from the true FSA dataset simulated in Field II. The second panel shows an image reconstructed from the FSA dataset recovered using regularized inversion ($\gamma = 0.001$), which achieves 0.9911 correlation with the ground truth. The next three panels show FSA images reconstructed from FSA datasets recovered from the walking aperture sequence at iterations 1, 30, and 60 of CG. The final plot show the correlation between the true and recovered FSA datasets as a function of the number of iterations of CG.

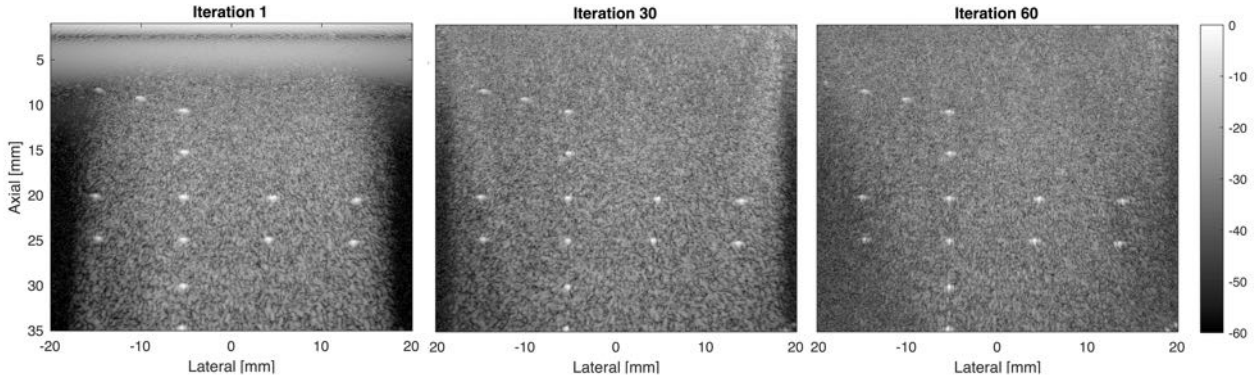

Fig. 2. Experiments in phantoms initially show strong artifacts close to the transducer surface and blind spots at the edges of the transducer, both of which disappear with each iteration. At 20 mm depth, resolution improves by 35% and 59% at iterations 30 and 60 of CG.

C. Full-Synthetic Aperture Image Reconstructions

The FSA image reconstructed from the FSA dataset recovered at each step of CG was compared to the FSA image reconstructed from the true FSA dataset. Furthermore, the walking aperture transmit sequence summarized in Table I was used to collect receive channel data from the L12-3v ultrasound probe on a CIRS 040GSE phantom. FSA datasets were recovered at each iteration of CG, and the corresponding FSA images were reconstructed. Resolution and spatial coherence [6] were quantified in the resulting images.

TABLE I
WALKING-APERTURE TRANSMIT SEQUENCE ON VERASONICS L12-3V

Parameter	Value	Units
Transmit Frequency	7.8130	MHz
Focal Depth	13.8	mm
Beam Origins	-19.1:0.2:19.1	mm
Aperture Width (Around Beam Origin)	25.2	mm

IV. RESULTS

A. Iterative Recovery of the FSA Dataset

Figure 1 shows the correlation between the true and recovered FSA dataset steadily increase with each iteration of CG. Initially, the reconstructed FSA images have poor resolution and a large amount of sidelobe clutter visible inside the anechoic lesion. However, as CG iterates through the transmit beamforming model and REFoCUS, the recovered FSA dataset becomes increasingly accurate and we observe the diffraction-limited resolution observable in the image reconstructed from the true FSA dataset. This indicates that the iterative recovery scheme reconstructs the signals for each single-element transmit so that FSA image reconstruction achieves complete transmit focusing at every point in the

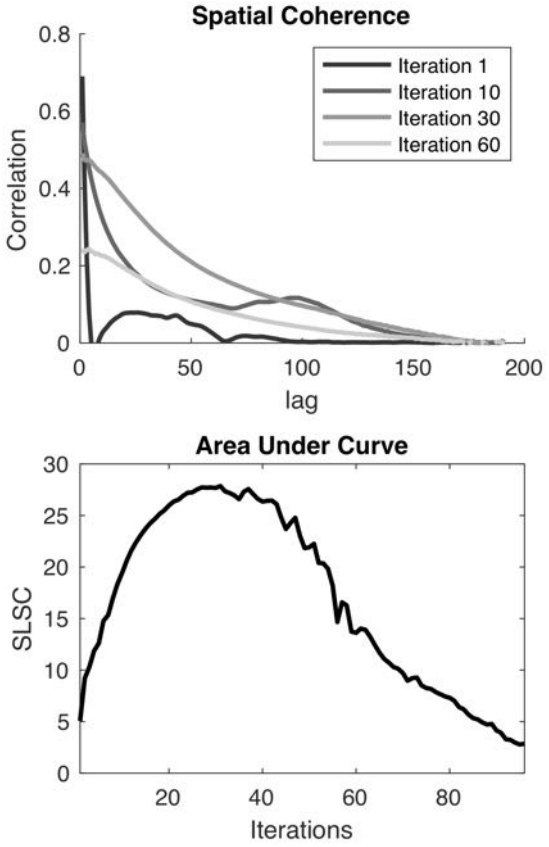

Fig. 3. Experiments in phantoms show that spatial coherence as a function of lag becomes increasingly triangular with each iteration of CG. However, due to the presence of noise, the lag-one coherence drops with each iteration. The short-lag spatial coherence (SLSC), or the area under the curve, is used to monitor this trade-off as function of the number of iterations. SLSC reaches its maximum at around 30 iterations of CG.

image.

B. Experimental FSA Image Reconstruction and Coherence

Experiments (Figure 2) show that direct applying REFoCUS (iteration 1) to received channel data results in near-field artifacts and blind spots at the edges of the field of view. By iteration 30, all near-field artifacts have disappeared and CG has begun to fill the blind spots. By iteration 60, we have also improved the lateral resolution of point targets in the medium. Figure 3 shows the spatial coherence of speckle recovered at each step of CG. Initially, the spatial coherence falls off rapidly as a function of lag. With each iteration of CG, the curve spatial coherence vs. lag becomes more triangular in shape, as expected by the VCZ theorem [6], [7]. However, the lag-one coherence also decreases as each iteration introduces noise into the recovered signal. In order to quantify this trade-off, the short-lag spatial coherence (SLSC) [6], which is simply the area under the coherence curve, was reported at each iteration. Although SLSC imaging typically relies on the variations in this value for contrast, we use SLSC as a quality metric for FSA dataset recovery in a uniformly diffuse-scattering medium. These results show that FSA dataset recovery no longer improves beyond 30 iterations for this particular walking aperture transmit sequence. In general, these results imply that CG may be stopped early to reduce computation time, and conserve signal-to-noise ratio.

V. Conclusions

Rather than directly model a single closed-form inversion operator, our approach leverages the adjointness of REFoCUS to recover the FSA dataset in an iterative manner. This approach supports both time and frequency domain implementations, and can potentially reduce the computational burden of FSA dataset recovery. Simulations demonstrate that the iterative scheme can recover the resolution and coherence expected in the true FSA dataset. Experiment show similar improvements in resolution, but reveal a key trade-off between the expected triangular shape of the coherence curve and the lag-one coherence. By monitoring the area under the coherence curve, we learn that CG should optimally be stopped after a certain number of iterations in order to maximally retain SNR and the triangularity of the spatial coherence curve. This early stopping of CG also presents an opportunity to reduce computation time.

Acknowledgment

Rehman Ali would like to thank the National Defense Science and Engineering Graduate (NDSEG) Fellowship for funding his graduate studies and research work. This work was also funded by NIH R01-EB017711 and R01-EB013361 from the National Institute of Biomedical Imaging and Bioengineering and the Duke-Coulter Translational Partnership Grant.

References

[1] M.-H. Bae and M.-K. Jeong, "A study of synthetic-aperture imaging with virtual source elements in b-mode ultrasound imaging systems," *IEEE transactions on ultrasonics, ferroelectrics, and frequency control*, vol. 47, no. 6, pp. 1510–1519, 2000.

[2] N. Bottenus, "Recovery of the complete data set from focused transmit beams," *IEEE transactions on ultrasonics, ferroelectrics, and frequency control*, vol. 65, no. 1, pp. 30–38, 2018.

[3] R. Ali, J. J. Dahl, and N. Bottenus, "Regularized inversion method for frequency-domain recovery of the full synthetic aperture dataset from focused transmissions," in *2018 IEEE International Ultrasonics Symposium (IUS)*. IEEE, 2018, pp. 1–9.

[4] P. Gong, M. C. Kolios, and Y. Xu, "Delay-encoded transmission and image reconstruction method in synthetic transmit aperture imaging," *IEEE transactions on ultrasonics, ferroelectrics, and frequency control*, vol. 62, no. 10, pp. 1745–1756, 2015.

[5] S. Diamond and S. Boyd, "Convex optimization with abstract linear operators," in *Proceedings of the IEEE International Conference on Computer Vision*, 2015, pp. 675–683.

[6] D. Hyun, A. L. C. Crowley, and J. J. Dahl, "Efficient strategies for estimating the spatial coherence of backscatter," *IEEE transactions on ultrasonics, ferroelectrics, and frequency control*, vol. 64, no. 3, pp. 500–513, 2016.

[7] R. Mallart and M. Fink, "The van cittert–zernike theorem in pulse echo measurements," *The Journal of the Acoustical Society of America*, vol. 90, no. 5, pp. 2718–2727, 1991.